Intelligence & Control
https://www.sciltp.com/journals/ic

Article

Multi Spherical Robot Control System for Nuclear Radiation Leak Detection

Xinyu He, Jianwen Huo * and Rui Lin

School of Information Engineering, Southwest University of Science and Technology, Mianyang 621000, China
* Correspondence: huojianwen2008@hotmail.com

How To Cite: He, X.; Huo, J.; Lin, R. Multi Spherical Robot Control System for Nuclear Radiation Leak Detection. *Intelligence & Control* **2025**, *1*(1), 2.

Received: 10 March 2025
Revised: 9 May 2025
Accepted: 7 July 2025
Published: 24 July 2025

Abstract: With the development of the global nuclear industry, the need for advanced safety and security measures has increased. Robotic systems have become a leading solution for detecting radioactive sources in nuclear power plants. However, a single robot often lacks flexibility and adaptability, especially in complex environments. To address these challenges, an innovative multi-spherical robot formation system based on the XK-I spherical robot platform, which is optimized for detecting nuclear leaks, is proposed in this paper. Firstly, this paper introduces an affine formation control algorithm, which supports formation maintenance, transformation, and scaling. Subsequently, an improved RRT* path planning algorithm is proposed, which ensures formation reliable path planning. These capabilities enable the multi-spherical robot system to autonomously inspect and detect nuclear power plant environments. Finally, based on theoretical analysis and calculations, a series of experiments are conducted to assess the ability of performing precise formation movements in nuclear power plants. The experimental results demonstrate that the multi-spherical robot control system can efficiently detect nuclear radioactive source leakage and achieve different formation motions accurately.

Keywords: multi-robot system; spherical robot; path planning; affine formation control; nuclear radiation leak detection

1. Introduction

The rapid development of nuclear energy, as an important part of the global energy mix, has placed higher demands on the safety of nuclear power plants. Nuclear leakage, whether triggered by equipment failure, natural disasters or human errors, may pose a serious threat to the environment and human health. Therefore, it is of great significance to develop an efficient and reliable nuclear leakage detection system.

In recent years, research on multi-robot systems has gained increasing attention and significance [1–3]. Multi-robot systems demonstrate flexible organizational structures, robust collaborative operation abilities, and high operational efficiency. Therefore, this paper proposes an innovative multi-spherical robot formation system based on XK-I spherical robot [4]. Compared to traditional wheeled, footed and drone-based nuclear operations robots, the greatest advantage of spherical robots applied in radiation source environment lies in that its special spherical shell can effectively disperse the external impact and radiation energy, so that the direct radiation impact on the internal electronic components and sensors is minimized. In addition, after the operation in the radiation source environment, the spherical shell makes it easy to decontaminate the radioactive source substances. Moreover, for nuclear power plants of different safety levels, the operation requirements can be realized by simply replacing the anti-radiation spherical shells of different levels. Considering the communication constraints among robots, we introduced graph theory concepts, enabling robots to achieve formation control by only communicating with their neighboring nodes.

Formation control is an important research component of time-varying formation control. It can be divided into the leader-follower method, virtual structure method, behavior-based method, consensus-based method, APF method and event-triggered method [5–10]. In recent years, distributed formation control methods based on graph theory have been widely studied. Dong et al. [11] investigated the formation control problem under switching interaction topologies. Lin et al. [12] introduced the stress matrix into the control of multi-robot systems, thereby forming affine formations. Zhao et al. [13] extended affine formations to arbitrary dimensional spaces and thus designed control laws. Building upon the affine theory, this study further explores the application of affine geometry in the formation control of spherical robots.

Reliable path planning algorithms are also essential for multi-robot systems. It can be classified into local path planning, heuristic search, intelligent search and sampling-based search. In this paper, we focus on enhancing the RRT*, which is a widely used sampling-based search algorithm.

The Rapidly-exploring Random Tree (RRT) was first introduced by Steven et al. [14] in 1998. RRT generates a tree structure through random sampling, avoids obstacles, and finds a path from the start to the goal. RRT does not need to model the planning space, but it has certain limitations, such as difficulty in identifying the optimal feasible path, high randomness, and low computational efficiency. To address these issues, researchers have proposed various improvements. Steven et al. [15] introduced the RRT* to optimize the feasibility of the path. Kuffner et al. [16] proposed the RRT-Connect algorithm to improve search efficiency. Additionally, Urmson et al. [17] proposed a target-biased RRT algorithm to reduce randomness. Building upon the goal-biasing approach, we incorporated this strategy into the RRT* algorithm to reduce path searching time. Furthermore, in complex environments with multiple robots and obstacles, the conventional RRT* algorithm only generates the shortest path without considering collision issues between the entire formation and obstacles. Thus, we introduced the artificial potential field concept to improve the RRT* algorithm, making it more suitable for the multi-robot multi-obstacle scenarios presented in this paper.

Based on the above analysis, this paper designs an affine transformation strategy and path planning algorithm in complex obstacle environments. Therefore, the main research contents of this paper are as follows:

(1) A multi-spherical robotic formation system for radioactive source detection is proposed, considering the complex environment of radioactive sources. In the event of a nuclear accident or other radioactive source leakage, such systems can be used to quickly monitor and assess the level of environmental contamination and enhance the efficiency of emergency response.
(2) This paper implements a multi-robot formation control algorithm considering the limitation of the communication range, and the robot only communicates with neighbouring robots.
(3) This paper introduces APF into the goal-biased RRT* path planning algorithm for multi-robot multi-obstacle environments, enabling the generation of reliable and effective formation traveling paths in such scenarios.

The paper is organised as follows. Section 2 introduces the kinematics model of spherical robots and the affine formation control strategy of multi-spherical robot system; Section 3 introduces the improved RRT* path planning algorithm; Section 4 introduces the experiments and results; The conclusion and future work are given in Section 5.

2. System Design

2.1. XK-I Spherical Robot Kinematics Model Analysis

The spherical robot structure studied in this paper consists of a spherical shell, a rectangular beam frame, a gravity pendulum, a vision system, and a control system circuit board. In addition, we integrate the radiation monitoring module MR-10-J to obtain the nuclear radiation dose information in real time and judge whether there is a risk of nuclear radiation leakage or not.

According to the structure of the spherical robot, the model is established to describe the movement mode of the spherical robot, the specific structure and coordinate system of XK-I spherical robot is shown in Figure 1 [4].

In the spherical robot coordinate system, (φ, β, ψ) is the X-Y-Z Euler angle. $\sum\{O_0, X_0\, Y_0, Z_0\}$ and $\sum\{O_1, X_1, Y_1, Z_1\}$ represent the inertial coordinate system fixed to the ground and the self-coordinate system of the geometric center of the sphere, respectively. R is the radius of the spherical robot, (X_C, Y_C) represents the position coordinates of the spherical robot under the ground inertial coordinate system. Then the pose matrix $q = [X_C, Y_C, \psi, \beta, \varphi]$ can be established. Suppose that the spherical robot rolls without sliding during the movement, the following constraint equation can be obtained according to the contact point between the spherical robot and the ground.

$$\begin{cases} \dot{X}_c - \dot{\varphi} R \cos\beta \sin\psi - \dot{\beta} R \cos\psi = 0 \\ \dot{Y}_c + \dot{\varphi} R \cos\beta \cos\psi - \dot{\beta} R \sin\psi = 0 \\ \dot{\psi} - \dot{\varphi} \sin\beta = 0 \end{cases} \tag{1}$$

When $\beta \neq \pi/2 \pm k\pi (k = 1,2 \ldots, n)$, the kinematic model of the spherical robot can be obtained as follows:

$$\begin{bmatrix} \dot{X}_c \\ \dot{Y}_c \\ \dot{\psi} \\ \dot{\beta} \\ \dot{\varphi} \end{bmatrix} = \begin{bmatrix} R\cos\psi & R\sin\psi\cos\beta \\ R\sin\psi & -R\cos\psi\cos\beta \\ 0 & \sin\beta \\ 1 & 0 \\ 0 & 1 \end{bmatrix} W(t) \tag{2}$$

In the above equation, $W = [\dot{\beta}, \dot{\varphi}]^T$ is the angular velocity of the spherical robot in both X and Y directions.

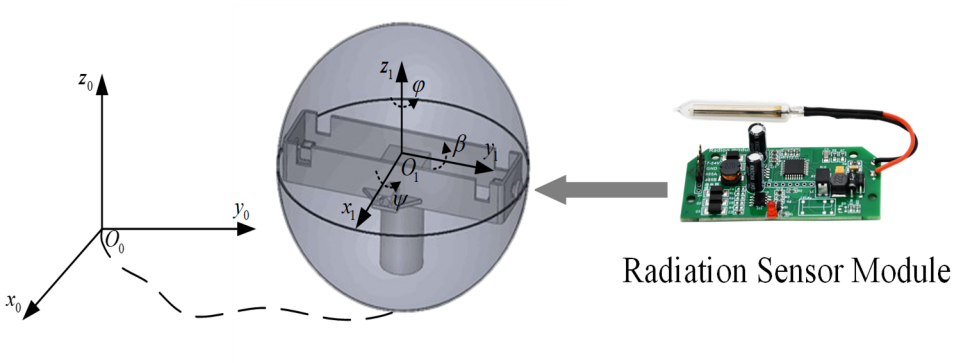

Figure 1. Structure and coordinate system of XK-I spherical robot.

2.2. Affine Formation Control Strategy for Multi-Spherical Robots

Affine transformation is widely used in the field of two-dimensional planar images, which is the superposition of linear transformation and translation transformation. For a multi-spherical robot formation, it can be regarded as a two-dimensional planar formation control. By introducing affine transformation, the state set of the multi-spherical robot network can be associated with the target configuration through an affine transformation, so that the time-varying formation can be described by an affine-equivalent formation. The changes of the nominal formation through affine transformation are shown in Figure 2, where (a) represents the nominal formation, (b) indicates the formation after the nominal formation is scaled, (c) is the formation after (b) is rotated, and (d) and (e) respectively stand for the formations after affine compression and rotation.

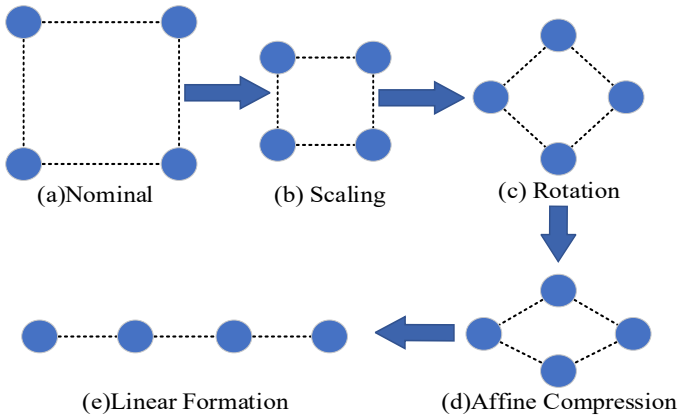

Figure 2. Examples of an affine transformation of the nominal formation.

Basic knowledge: A multi-spherical robot formation can be regarded as the formation control in a two-dimensional plane. We employ the stress matrix to design an undirected communication topology. Establish a swarm system composed of n spherical robots in the two-dimensional space while the relationship between spherical robots can be described by $\mathcal{G} = (\mathcal{V}, \mathcal{E})$ which consists of an edge set $\mathcal{E} \subseteq \mathcal{V} \times \mathcal{V}$ and a vertex set $\mathcal{V} = \{1, \cdots, n\}$. The setting of edges and vertices composes the communication topology graph. Where $\mathcal{V}_i$ represents

robot i and the edge $(i,j) \in \mathcal{E}$ indicates that robot i and robot j are neighbors and can realize information interaction, which means $(i,j) \in \mathcal{E} \Leftrightarrow (j,i) \in \mathcal{E}$.

Denote $(\mathcal{G},p)$ as the multi-spherical robot formation. Suppose that the first n_l spherical robots are leaders and the rest $n_f = n - n_l$ robots are followers. $\mathcal{V}_l = \{1,\cdots,n_l\}$ and $\mathcal{V}_f = \mathcal{V}\backslash\mathcal{V}_l$ are respectively the sets of leaders and followers, and their real-time positions are recorded as $p_l = \left[p_1^T,\cdots,p_{n_l}^T\right]^T, p_f = \left[p_{n_{l+1}}^T,\cdots,p_n^T\right]^T$.

For the spherical robot formation $(\mathcal{G},p)$, $\{\omega_{ij}\}_{(i,j)\in\mathcal{E}}$ is the stress weight on the edge (i,j) and $\omega_{ij} = \omega_{ji}$. The structure of the stress matrix is determined by the topology graph and the value of the matrix is determined by the formation shape. For any affine transformation of the swarm, its stress matrix remains unchanged. At the same time, the equilibrium stress should satisfy $\sum_{j\in\mathcal{N}_i}\omega_{ij}(p_j - p_i) = 0, i \in \mathcal{V}$, and the equilibrium stress matrix can be expressed as:

$$[\Omega]_{ij} = \begin{cases} 0, & i \neq j, (i,j) \notin \mathcal{E} \\ -\omega_{ij}, & i \neq j, (i,j) \in \mathcal{E} \\ \sum_{k\in\mathcal{N}_i}\omega_{ik}, & i = j \end{cases} \tag{3}$$

We take seven spherical robots as an example to design the formation control system and design the topology graph of nominal formation for seven spherical robots as shown in Figure 3:

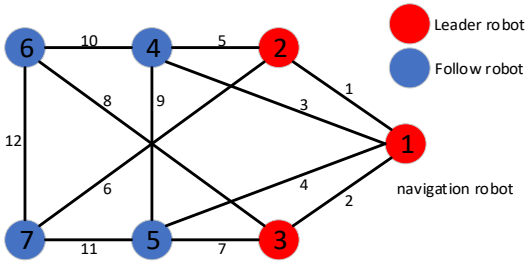

Figure 3. Topology graph of nominal formation for seven spherical robots.

The time-varying formation form of the nominal formation under affine transformation is as follows:

$$p^*(t) = [I_n \otimes A(t)]r + 1_n \otimes b(t) \tag{4}$$

where $A(t) \in R^{2\times 2}$ and $b(t) \in R^2$ respectively represent the linear transformation and translation transformation of the formation, and both are continuous of t while t is the parameter of time. $p_l = \left[p_1^T,\cdots,p_{n_l}^T\right]^T, p_f = \left[p_{n_l+1}^T,\cdots,p_n^T\right]^T$ is a constant configuration of the nominal formation. $I_n \in R^{n\times n}$ and $1_n \in R^n$ are the identity matrix and vector with all entries equal to one, respectively. Then we quote the formation control law of the time-varying leaders' velocities under single-integrator agent dynamics [13] as follows.

$$\dot{p}_i = -\frac{1}{\gamma_i}\sum_{j\in\mathcal{N}_i}\omega_{ij}\left[(p_i - p_j) - \dot{p}_j\right], \quad i \in \mathcal{V}_f \tag{5}$$

where $\gamma_i = \sum_{j\in\mathcal{N}_i}\omega_{ij}$. As a result, we just need to plan the path of the leading robots and control the following robots through the control law to realize the functions such as maintaining and transforming the formation.

3. Improved RRT* Algorithm for Path Planning

Initially, the Goal-Biased RRT* algorithm was employed in global path planning. However, experimental findings reveal that, during the iteration of optimal paths, the generated paths frequently became too close to the obstacles. Consequently, APF is introduced to ensure the safety of the formation, not merely the paths of the leader robot.

The pseudocode of the improved RRT* algorithm is shown in Algorithm 1, where M and n are the known static map and the number of iterations, respectively. q_{start} and q_{goal} represent the start and end points of the random tree in the map, respectively. Initialisation of the search tree is the first step. Secondly, given a target bias probability threshold $p_{threshold}$ between 0 and 1, q_{rand} is randomly generated on the map when $p > p_{threshold}$; q_{rand} is equal to q_{goal} when $0 < p \leq p_{threshold}$. The fifth step involves identifying the nearest node to q_{rand} in the tree, which is q_{nearst}. In steps 6 and 7, APF is employed to generate a new node (q_{new}), and updating q_{new} by extending it from q_{nearst} to q_{new} by one stepsize. The eighth step in the process is to consider the extension of the tree in the absence

of obstacles. Finally, reselection of parent nodes and resampling operations are performed in steps 9 and 10, respectively.

Algorithm 1 Improved RRT* Algorithm

Input: M, q_{start}, q_{goal}
Result: A path from q_{start} to q_{goal}

1. $Tree \leftarrow Initializetree();$
2. $Tree \leftarrow InsertNode(\emptyset, q_{start}, Tree);$
3. $For\ i = 0\ to\ n\ do$
4. $If\ p > p_{threshold}\ then$
$q_{rand} \leftarrow Sample(M);$
$else$
$q_{rand} = q_{goal};$
end
5. $q_{nearest} \leftarrow Nearest(Tree, q_{rand});$
6. $q_{new} \leftarrow APF\ \ newpoint(q_{rand}, q_{nearest}, Obstacle);$
7. $q_{new} \leftarrow Extend(q_{nearest}, q_{new}, stepsize)$
8. $If\ Obstaclefree(q_{nearest}, q_{new})\ then$
$InsertNode(Tree, q_{new})$
$Insertedge(q_{nearest}, q_{new})$
9. $Q_{near} \leftarrow Near\_neighbors(Tree, q_{new}, r)$
$If\ Obstaclefree(Q_{near}, q_{new})\ then$
$q_{min} \leftarrow Chooseparent(Q_{near}, q_{new})$
$Insertedge(q_{nearest}, q_{min})$
10. $Tree \leftarrow Review(T, q_{near}, q_{min}, Tree)$
11. $End\ if$
12. $End\ for$
$End\ Tree$

The concept of obstacle repulsion in APF is introduced into the RRT* algorithm to guide the local random tree to grow away from obstacles. The schematic diagram is shown in Figure 4. In this study, the gravitational force function of q_{rand} and the repulsive force function of obstacles are denoted as $U_{att}(x)$ and $U_{rep}(x)$, respectively. The generation of q_{new} is based on $F(x)$, which can be expressed as Equation (6).

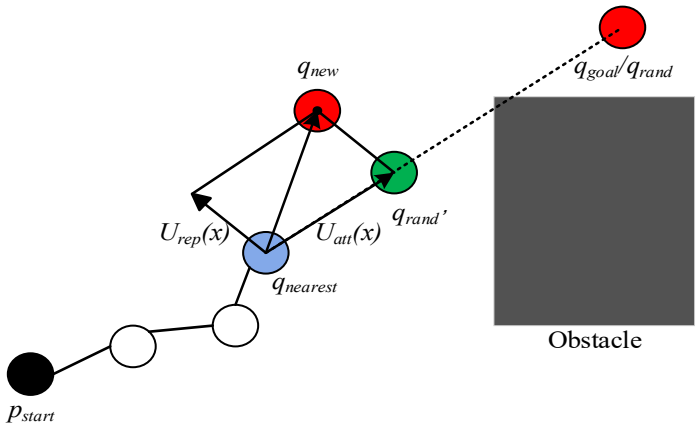

Figure 4. Schematic diagram of the APF for generating q_{new}.

$$F(x) = U_{att}(x) + U_{rep}(x) \tag{6}$$

$$U_{att}(x) = \rho \times k_{att} \times \frac{x_{rand} - x_{nearest}}{|x_{rand} - x_{nearest}|} \tag{7}$$

$$U_{rep}(x) = \begin{cases} 0, d(x) > R \\ \rho k_{rep} \left(\frac{1}{d(x)} - \frac{1}{R}\right) \frac{1}{d(x)^3} \frac{x_{obstacle} - x_{nearest}}{|x_{obstacle} - x_{nearest}|}, d(x) \le R \end{cases} \tag{8}$$

As illustrated in Equations 7 and 8, $U_{att}(x)$ and $U_{rep}(x)$ are shown respectively. The step size is denoted by ρ, whilst k_{att} and k_{rep} represent the respective values of the gravitational coefficient and the coefficient of repulsion of the obstacle. The position vectors of q_{rand} and q_{nearst} are indicated by X_rand $x_{rand}$and $x_{nearest}$ respectively. The distance from the obstacle to q_{nearst} is denoted by $d(x)$. R is the maximum range at which the obstacle affects the spherical robot, and $x_{obstacle}$ is the position vector of the obstacle.

4. Experiments

To illustrate the feasibility of the proposed improved RRT* algorithm and the formation control system, MATLAB is used to build the simulation environment. A simulation map (100 × 100) was created. The step size is 3, the maximum number of iterations is 1000, and each group of experiments is run 50 times to obtain the mean value. The starting point (1,1) and the goal point (100,100) are marked in pink and green, respectively.

To determine the value of $p_{threshold}$, we conducted comparative experiments with different $p_{threshold}$ value (0.1, 0.2, ..., 0.5), and the results are shown in Table 1. The experimental results indicate that when the $p_{threshold}$ increases from 0.1 to 0.3, it can accelerate the map exploration rate. However, when the $p_{threshold}$ increases from 0.3 to 0.5, an excessively high $p_{threshold}$ may cause the generated tree to be formed inside obstacles, leading to wasted exploration and consequently prolonged exploration time. Finally, we determined that 0.3 was adopted as the value of $p_{threshold}$.

Table 1. Performance comparison results of different $p_{threshold.}$

$p_{threshold}$	**0.1**	**0.2**	**0.3**	**0.4**	**0.5**
Average experiment time(s)	1.331	0.985	0.7270	0.7598	0.7903
Average path length	165.682	168.176	164.859	166.304	165.063
Average iteration	295.660	245.880	213.060	262.540	290.900

To verify the reliability of the improved RRT* algorithm after introducing APF, we conducted comparative experiments before and after the introduction, as shown in Figure 5, which shows that the improved RRT* algorithm with APF can maintain a better distance from obstacles, thereby ensuring the safety of the entire formation. This thus proves both the feasibility and necessity of introducing APF method.

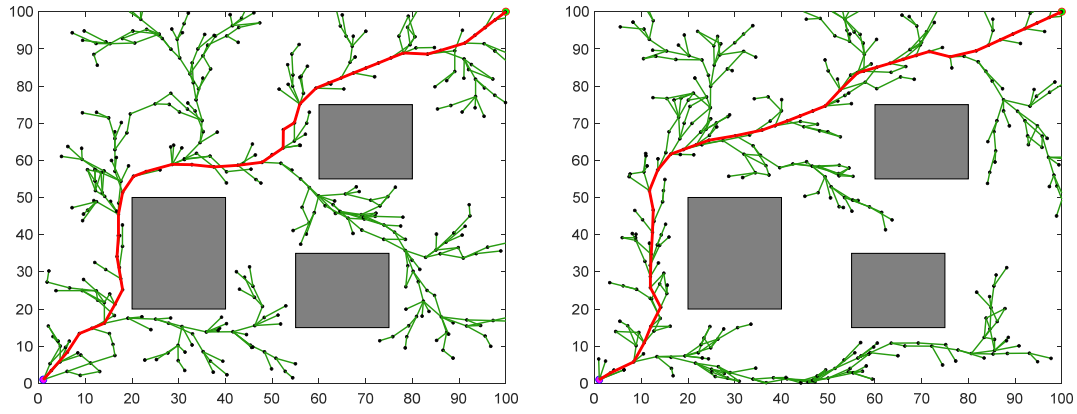

Figure 5. Comparison of experimental results before and after the addition of APF.

To verify the proposed formation control system, a 100m*100m simulation environment was constructed to model a simplified nuclear power plant. The starting coordinates of the seven spherical robots are: $\begin{bmatrix} 5 & 2.5 & 6.5 & 1 & 6 & 0 & 5 \\ 5 & 3.5 & 2.5 & 2.5 & 1 & 1 & 0 \end{bmatrix}$, the starting point and goal point of the leader robot are (5, 5) and (95, 95), respectively. Several obstacles were added, and a linear segment path was manually set considering the specificity of the passage. The original parameters were retained for path planning. It is evident that the RRT* algorithm generates paths that are connected by line segments, which can cause large motion errors and increase energy loss. So we employ the Bézier curve to smooth the paths, thus reducing the motion errors. The final planned global route is shown in Figure 6.

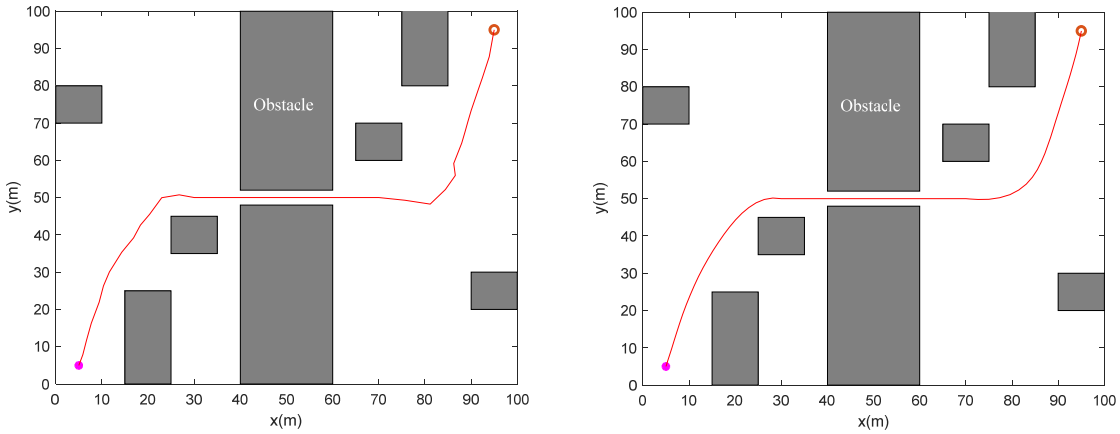

(a) Global path planned by improved RRT* algorithm **(b) Global path after Bézier curve optimisation**

Figure 6. Experimental Results of Path Planning.

To verify the feasibility of radiation source detection, a simulated radiation source following a Poisson distribution is added at the target location to construct a radiation field. The formation obstacle avoidance simulation trajectory is shown in Figure 7. The corresponding tracking error, as well as the time-varying velocity in the X-axis and Y-axis, are shown in Figures 8–10, respectively.

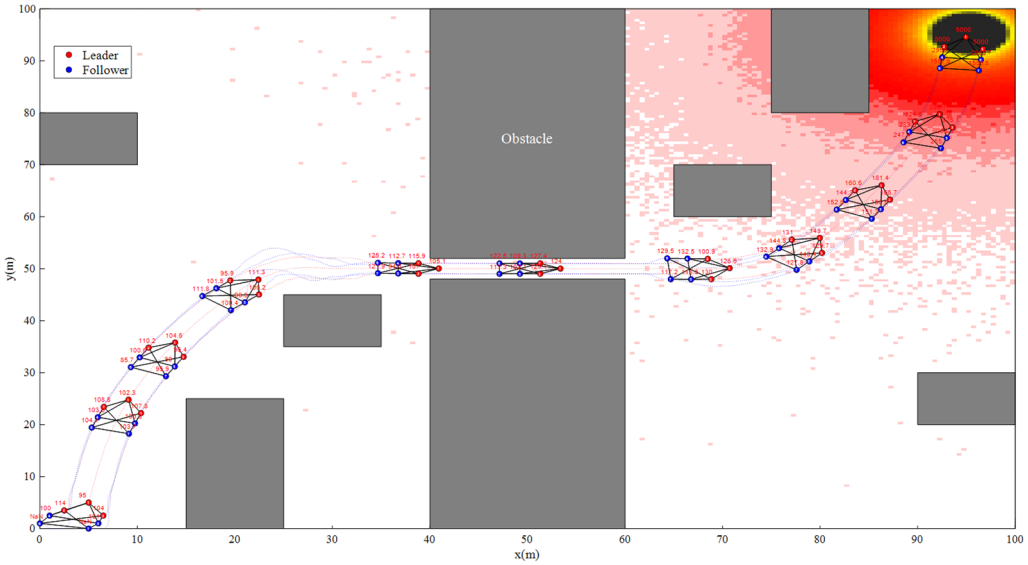

Figure 7. Simulation diagram of formation trajectory.

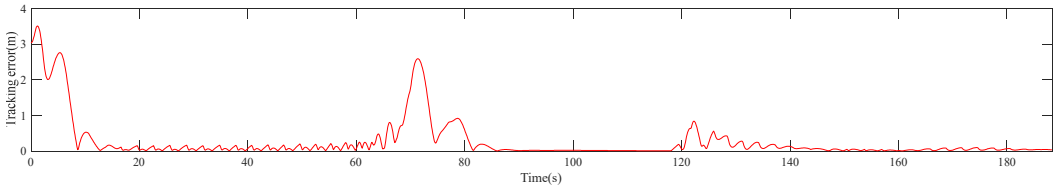

Figure 8. Tracking position error.

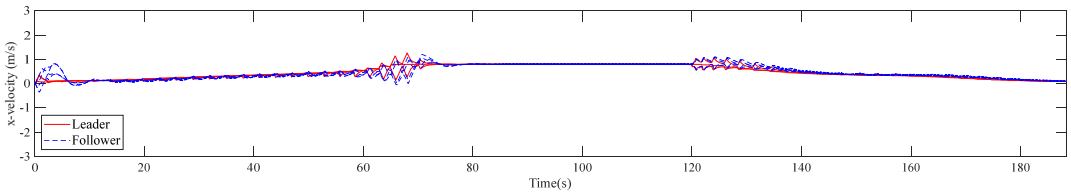

Figure 9. Time-varying velocity in the X-axis.

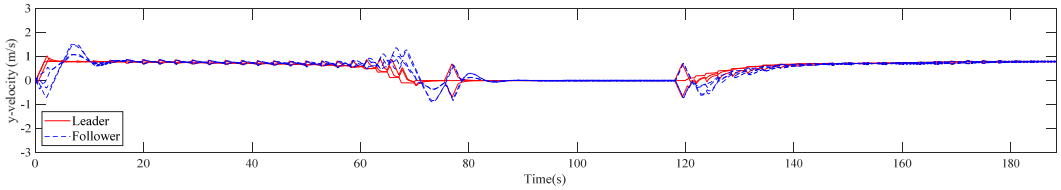

Figure 10. Time-varying velocity in the Y-axis.

Just as demonstrated in Figure 7, the multi-spherical robot formation starts at random positions, moves along the planned path, bypasses obstacles and ultimately reaches the destination. Additionally, it can display the detected radiation dose in real-time.

Figure 8 demonstrates the overall formation tracking error, showing three fluctuations. The first occurred at 0–10 s: since the robots' initial positions were randomly assigned, which required time to converge to the formation. The second and third fluctuations occurred at 68–80 s and 120–140 s, respectively, both triggered by simultaneous sharp turns and formation scaling/expansion. Additionally, the lack of formation speed constraints during movement exacerbated these three tracking errors—note that these errors were not caused by the algorithm itself or simulation setup. Mitigation strategies include: reducing sharp turns in the planned path, and limiting formation speed during turns or formation changes to minimize tracking errors. As demonstrated in Figures 9 and 10, the velocity of spherical robots exhibits no substantial fluctuations along the X-axis and Y-axis.

5. Conclusions and Future Work

This paper has presented a multi-spherical robot control system for the detection of nuclear radiation source leakage in nuclear power plants. The system has two main functions: decision-making and execution capabilities. An affine formation control method based on graph theory and stress matrices is proposed, which enables the formation to perform scaling, rotation, and shearing transformations in a two-dimensional plane. Each spherical robot can independently determine its actions based solely on the information from its neighbouring nodes. The improved RRT* algorithm generates reliable paths by utilizing environmental information. The formation system can follow the planned route and bypass obstacles, such as narrow passages and ultimately reach the target point. Additionally, the system provides real-time detection data of radiation dose, effectively fulfilling the detection tasks, and the collected data can serve as experimental support for radiation source estimation and related research.

Future work will focus on transferring the system from a simulated environment to real-world nuclear radiation source detection scenarios. To address this, we will formulate local path planning strategies to cope with possible dynamic obstacles and propose a radiation source positioning method during movement, to achieve precise identification and localization of radiation sources. Other potential issues include but are not limited to sensor accuracy, communication delay, and battery life. For sensor accuracy issues, we can improve the positioning effect when sensor accuracy is insufficient by fusing multi-sensor data through Kalman filtering in a multi-robot collaborative manner. For communication delays, we can initially solve the problem by strengthening the radiation hardening of semiconductor components to ensure that robots can operate longer in radiation environments. For the robot battery life issue, an adaptive sleep mechanism will be proposed to reduce the sampling frequency in low-radiation areas, thereby reducing the power consumption of sensors.

Author Contributions

X.H.: conceptualization, methodology, software, writing—original draft preparation; J.H.: data curation, investigation, supervision; R.L.: validation, writing—reviewing and editing. All authors have read and agreed to the published version of the manuscript.

Funding

This research was funded by the National Natural Science Foundation of China (No. 12205245).

Institutional Review Board Statement

Not applicable.

Informed Consent Statement

Not applicable.

Data Availability Statement

The authors confirm that the data supporting the findings of this study are available within the article.

Acknowledgments

The authors gratefully acknowledge anonymous editors and reviewers.

Conflicts of Interest

The authors declare no conflict of interest. The funders had no role in the design of the study; in the collection, analyses, or interpretation of data; in the writing of the manuscript; or in the decision to publish the results.

References

1. Ristic, B.; Angley, D.; Moran, B.; et al. Autonomous multi-robot search for a hazardous source in a turbulent environment. *Sensors* **2017**, *17*, 918.
2. Li, B.; Zhu, Y.; Wang, Z.; et al. Use of multi-rotor unmanned aerial vehicles for radioactive source search. *Remote Sens.* **2018**, *10*, 728.
3. Luo, M.; Huo, J.; Liu, M.; et al. Distributed collaboration: Cognitive difference and collaborative decision for multi-robot radioactive source search. *Ann. Nucl. Energy* **2024**, *196*, 110210.
4. Liu, M.; Lin, R.; Yang, M.; et al. Active disturbance rejection motion control of spherical robot with parameter tuning. *Ind. Robot Int. J. Robot. Res. Appl.* **2022**, *49*, 332–343.
5. Ni, J.; Shi, P. Adaptive neural network fixed-time leader–follower consensus for multiagent systems with constraints and disturbances. *IEEE Trans. Cybern.* **2020**, *51*, 1835–1848.
6. Moreira, M.S.M.; Villa, D.K.D.; Sarcinelli-Filho, M. Controlling a Virtual Structure Involving a UAV and a UGV for Warehouse Inventory. *J. Intell. Robot. Syst.* **2024**, *110*, 121.
7. Lee, G.; Chwa, D. Decentralized behavior-based formation control of multiple robots considering obstacle avoidance. *Intell. Serv. Robot.* **2018**, *11*, 127–138.
8. Ma, N.; Cao, Y. Consensus-based distributed formation control for coordinated battle system of manned/unmanned aerial vehicles. *Trans. Inst. Meas. Control* **2024**, *46*, 3–14.
9. Chen, H.; Chen, H.; Qiang, L. Multi-UAV 3D formation path planning based on improved artificial potential field. *J. Syst. Simul.* **2020**, *32*, 414–420.
10. Li, Y.; Dong, S.; Li, K. Fuzzy adaptive finite-time event-triggered control of time-varying formation for nonholonomic multirobot systems. *IEEE Trans. Intell. Veh.* **2023**, *9*, 725–737.
11. Dong, X.; Zhou, Y.; Ren, Z.; et al. Time-varying formation tracking for second-order multi-agent systems subjected to switching topologies with application to quadrotor formation flying. *IEEE Trans. Ind. Electron.* **2016**, *64*, 5014–5024.
12. Lin, Z.; Chen, Z.; Fu, M. A linear control approach to distributed multi-agent formations in d-dimensional space. In Proceedings of the 52nd IEEE Conference on Decision and Control, Firenze, Italy, 10–13 December 2013; pp. 6049–6054.
13. Zhao, S. Affine formation maneuver control of multiagent systems. *IEEE Trans. Autom. Control* **2018**, *63*, 4140–4155.
14. LaValle, S.M.; Kuffner, J.J. Rapidly-exploring random trees: Progress and prospects. In *Algorithmic and Computational Robotics*; CRC Press: Boca Raton, FL, USA, 2001; pp. 303–307.
15. Karaman, S.; Walter, M.R.; Perez, A.; et al. Anytime motion planning using the RRT. In Proceedings of the 2011 IEEE International Conference on Robotics and Automation, Shanghai, China, 9–13 May 2011; pp. 1478–1483.
16. Kuffner, J.J.; LaValle, S.M. RRT-connect: An efficient approach to single-query path planning. In Proceedings of the IEEE International Conference on Robotics and Automation. Symposia Proceedings (Cat. No. 00CH37065), San Francisco, CA, USA, 24–28 April 2000; pp. 995–1001.
17. Urmson, C.; Simmons, R. Approaches for heuristically biasing RRT growth. In Proceedings of the 2003 IEEE/RSJ International Conference on Intelligent Robots and Systems (IROS 2003) (Cat. No. 03CH37453), Las Vegas, NV, USA, 27–31 October 2003; pp. 1178–1183.